THE MSFC VECTOR MAGNETOGRAPH

M. J. HAGYARD, N. P. CUMINGS, E. A. WEST, and J. E. SMITH

Space Sciences Laboratory, NASA Marshall Space Flight Center, Marshall Space Flight Center, Ala. 35812, U.S.A.

(Received 28 September; in revised form 21 December, 1981)

Abstract. The NASA/Marshall Space Flight Center's solar vector magnetograph system is described; this sytem allows measurements of all components of the Sun's photospheric magnetic field over a 5 × 5 or 2.0 × 2.0 arc min square field-of-view with an optimum time resolution of ~ 100 s and an optimum signal-to-noise of ~ 1600. The basic system components are described, including the optics, detector, digital system and associated electronics. Automatic sequencing and control functions are outlined as well as manual selections of system parameters which afford unique system flexibility. Results of system calibration and performance are presented, including linearity, dynamic range, uniformity, spatial and spectral resolutions, signal-to-noise, electro-optical retardation and polarization calibration. Scientific investigations which utilize the unique characteristics of the instrument are described and typical results are presented.

1. Introduction

The NASA/Marshall Space Flight Center (MSFC) vector magnetograph system originated as a joint effort between the Naval Research Laboratory (NRL) and MSFC, and the original design of the instrument was the concept of Dr Guenther Brueckner (NRL). This magnetograph possesses the unique capability of measuring *very rapidly* (within 100 s) the full magnetic vector over an entire active region with good spatial resolution (~ 3.3 arc sec) and with sufficient sensitivity to detect ~ 4 G line-of-sight (longitudinal) fields and ~ 70 G transverse fields. In this paper we present a description of the system, discuss its calibration and performance characteristics, and describe some of the specific scientific investigations which are uniquely applicable to this instrument.

2. System Description

The measurement of solar vector magnetic fields with the MSCF magnetograph is based on the interpretation of observations of linearly and circularly polarized intensities of a Zeeman-sensitive absorption line selected by a narrow-bandpass birefringent filter. The primary components of the magnetograph are the optical system (light collector, polarization analyzer and filter), camera system, digital system and associated electronics.

2.1. Optical System

The optical train of the MSFC vector magnetograph is shown in Figure 1. Attached to the front of a 30 cm Cassegrainian telescope is a full-aperture prefilter with a half width of 21 nm centered at 525 nm and peak transmission of 65% at 525 nm. The $f/13$ Cassegrainian telescope focus, with an image diameter of 3.5 cm, is at a mirrored aperture stop which limits the field of view of the Sun to 5 by 5 arc min and reflects the unused

Solar Physics **80** (1982) 33–51. 0038–0938/82/0801–0033$02.85.

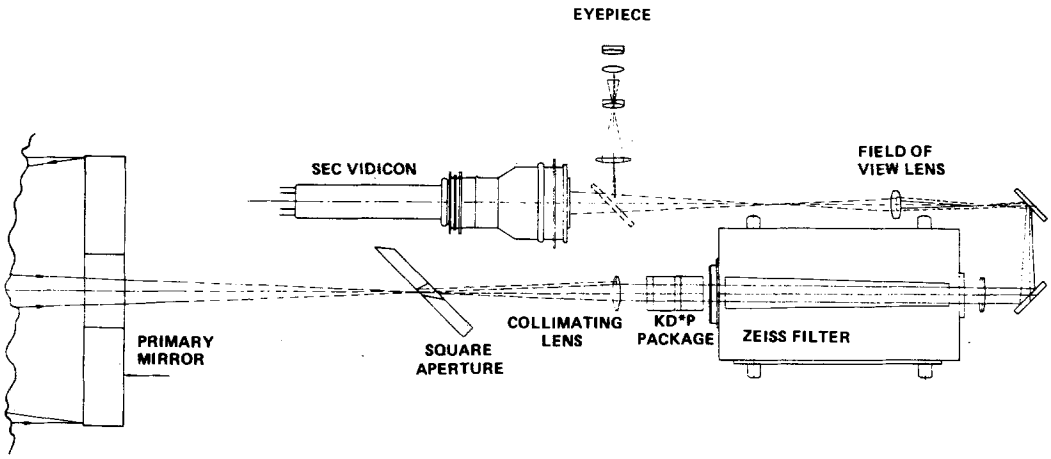

Fig. 1. Schematic diagram of the optical system.

image into the correlation tracker optics. Following the aperture stop is a collimating lens that insures that the cone angle for the beam passing through the polarizing optics is smaller than 2 degrees. The polarizing optics consist of two KD*P (potassium deuterium phosphate) crystals, a MgF_2 (magnesium fluoride) crystal, and a Zeiss birefringent filter. The KD*P crystals are used as variable waveplates, and the MgF_2 crystal is used to extend the acceptance angle of the two KD*P crystals to 2 degrees. The first polarizing element of the Zeiss birefringent filter is used as the analyzer of the system. The Zeiss filter is a 0.0125 nm bandwidth filter centered on the Fe I line, 525 nm, and can be tuned $\pm$ 0.800 nm. The light transmitted by the Zeiss filter is folded around the optics box and through a lens system consisting of two independent and exchangeable magnification systems which refocus a 5 by 5 arc min or 2.0 by 2.0 arc min field of view of the Sun onto a Secondary Electron Conduction (SEC) vidicon tube.

2.2. Camera System

The camera system consists of an SEC detector, associated signal conditioning electronics, and the system memory; a block diagram is shown in Figure 2.

2.2.1. *Detector*

The selected field of view is imaged by the optics on an SEC camera tube with a fiber optics faceplate. The useful diameter of the tube is 40 mm, allowing a 28 $\times$ 28 mm image to be formed. The tube consists of an S-20 photocathode, an electrically focused diode image section, an SEC target and a magnetically focused and deflected reading section. Horizontal and vertical alignment coils located in the deflection assembly can be variably controlled to select the optimal area of the vidicon target. The magnetically deflected read beam scans the SEC target in 128 discrete horizontal steps along 128 discrete lines.

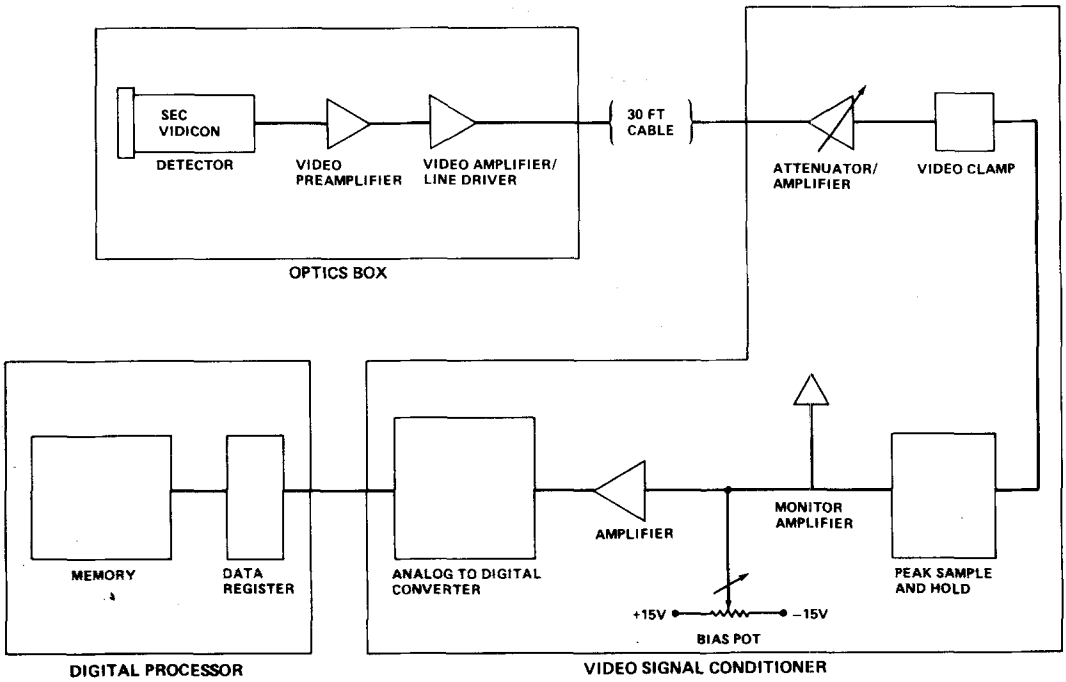

Fig. 2. Block diagram of the camera system.

2.2.2. *Electronics*

The signal from the SEC tube is coupled directly into a video pre-amplifier which was designed specifically to match the SEC vidicon tube characteristics and to reduce output noise. A ten-step amplifier is used to adjust the video signal to the optimum level required by the digitizing electronics. The optimized signal passes into a dc restoration circuit consisting of a keyed clamp and a wideband video amplifier. The clamp keeps the dc level of the data at zero volts so that there is no smearing between picture elements under extreme contrast conditions.

A peak sample and hold circuit retains the peak value of each picture element for 1.2 μs to allow a complete conversion of the analog signal into an 8-bit digital word by the analog-to-digital converter with a resolution of one part in 256.

The output of the a/d is fed into the system memory which is used for data storage and pre-processing. This memory has a capacity of 16 K × 32 bits, a 275 ns access time and can store two 128 × 128 images (A, B) simultaneously. Typically, a stored image is built up by adding, pixel by pixel, successive images (up to a maximum of 255); the stored image word size is variable from 8 to 16 bits depending on the number of images which are superimposed. Selector switches allow the display of either A or B or of the image produced from the subtraction (A–B).

2.3. Sequencing and Control Electronics

The sequencing and control of the magnetograph is directed by a controller which provides all timing signals, sync pulses, and driver and control logic. In addition to these

functions, the controller also affords flexibility by providing for the automatic selection by the operator of various system parameters as discussed in the following subsections.

2.3.1. *Dynamic Range*

Variation of the photocathode voltage of the SEC tube provides a gain control range of 15 : 1; additional system dynamic range can be obtained by changing the exposure times and attenuator/amplifier settings: six exposure times can be selected ranging from 1/60 s to 1/1.875 s, and the attenuator/amplifier has ten steps, each changing the signal gain by 10%.

2.3.2. *Image Enhancement*

To obtain an increased signal-to-noise ratio the data can be digitally enhanced by a process of superimposing successive images from N polarization pairs (A, B) in the two memory registers, where N can be varied in one-step intervals from 1 to 255. Operating at 1/60 s exposure duration, the full 255 enhancements of a polarization pair (A, B) can be obtained and recorded in 35 s.

2.3.3. *Filter Wavelength Selection*

Using selector switches, the operator can tune the Zeiss birefringent filter over a wavelength interval 525 ± 0.5 nm in steps of 0.001 nm. Control is provided by four independent thumbwheel switches so that four different filter positions can be pre-programmed and quickly selected.

2.3.4. *Polarization Analysis Sequences*

The operator can select five different polarization analysis operations of the KD*P modulators which provide the options of measuring the longitudinal magnetic field, transverse field or vector field.

2.3.5. *SEC Target Signal Retention*

To reduce errors introduced by beam-discharge lag, the sequencing and control electronics can be pre-set so that the vidicon is re-scanned by the read beam without target exposure. This re-scan without exposure can be performed up to 7 times; however, 1 re-scan is usually sufficient, and over-erasure can charge the target negatively, with a resulting reduced signal in the next exposure (Honeycutt and Burkhead, 1973; Walker *et al.*, 1972).

A different target characteristic of the SEC which can introduce errors into the data is the presence of image charge patterns within the area of the SEC target which are not completely neutralized as the readout beam is swept across the target in discrete steps. If the SEC vidicon is not operated for a time interval of several seconds, or longer, these charges will 'bleed' laterally, recharging the target area previously discharged by the readout beam. As a result the target signal of the first exposure of the next data set may be up to 10% greater than subsequent signals. To circumvent the problem the control

electronics have been modified to automatically reject the first exposure in the *A* and *B* frames so that these data are not put into the memory.

2.4. Data Recording and Storage

The magnetograph system uses a microcomputer to process data stored in the microram memory. These data are initially stored on a 5-megabyte cartridge disk; once data acquisition is complete, the data are transferred to magnetic tape for permanent storage and input to other computers for data reduction and analysis. The tape recorder is a nine-track recorder with ping-pong buffers of 16 K bit capacity each of which can store data at a 1 Mbit s^{-1} rate; transfer time to magnetic tape is about 10 s per image.

2.5. Auxiliary Systems

2.5.1. *Test Pattern Generator*

A digital signal generator is provided in the system which produces 16 levels of grey, each one-half of the amplitude of the preceding level and equally spread across the tube format. The generator is capable of producing the grey levels in either horizontal or vertical bars, or a flat field can be produced at the 16 greyscale levels.

2.5.2. *Solar Guider*

The solar tracking system for the MSFC magnetograph consists of a Sun sensor, torque motor drivers and associated electronics. The Sun sensor is a two-axis sensor using two detectors for each axis and a fifth detector as an intensity sensor for automatic gain control (AGC). The sensor field of view is $\pm 6°$ with a nonlinearity of approximately 1% over the range of $\pm 0.5°$. The sensor can point the telescope to any given spot on the Sun as the operator dials in an offset voltage; the AGC maintains the position regardless of changes in intensity. The combined nonlinearity of the AGC and the sensor fix the accuracy of defining or locating a spot to about 15 arc sec. The jitter stability about any spot with little or no wind is about ± 2 arc sec.

2.5.3. *Correlation Tracker*

Frequently, wind conditions at the MSFC observing site produce significant high-frequency oscillations which the guider system cannot accommodate. To stabilize these motions a solar correlation tracker has been integrated into the magnetograph system. This correlation tracker compensates for image motion using error signals derived from a video correlation technique; the error signals drive a flat optical element to translate the image to the original unperturbed position. Tests have been conducted with this instrument in operation during magnetograph observations to assure that no spurious linear polarization is introduced into the data by the flat plate.

3. System Calibration and Performance

Prior to installing the SEC vidicon which is presently in operation in the magnetograph, an extensive testing program was conducted in order to document its performance in the

system. In Sections 3.1 through 3.7 we discuss results of these tests, in Section 3.8 we discuss performance characteristics of the Zeiss filter, and in Sections 3.9 and 3.10 we present results of polarization analyses and calibrations.

3.1. Linearity

The characteristics of the tube were measured to insure that the vidicon is operated in the linear portion of its transfer curve which relates signal output current to signal input (photons received). The light source used in this test was a calibrated optoliner with a set of neutral density filters to provide accurately known light levels at the SEC faceplate. The resulting output signal current was measured for each increment of attenuation; the measured current was the envelope of the composite signal from the central portion of the tube. The data indicate that the transfer curve is linear for tube operation at a signal current output less than 100 nA. In normal operation, the high-voltage power supply for the vidicon is adjusted such that maximum solar illumination corresponds to $\sim$ 100 nA; consequently, all intensity variations from photospheric to umbral levels measured over the field of view fall on the linear portion of the transfer curve.

To test the linear response of the system apart from the vidicon, the greyscale generator described in Section 2.5.1 was used. Following tests to assure the linearity of the generator, data were obtained for system response to the 16 greyscale levels as a function of a/d bias. Results indicated a linear response over an a/d bias range 0.30–1.30. In normal operations the a/d bias value is selected so that any dc voltage unrelated to the signal is not digitized.

3.2. Dynamic range

The range of illumination which can be accommodated by the tube within a single scene is roughly from 10^{-5} to 10^{-3} footcandle (within the linear portion of the light transfer curve). The dynamic range of the complete system is determined by the overall signal-to-noise of the system, which is $\sim$ 100 : 1 (see Section 3.7); this value provides more than sufficient range to accommodate the radiance variations in a solar scene which range from umbral to photospheric intensities.

3.3. Geometrical distortion

The geometrical distortion of the vidicon was investigated by illuminating the faceplate with a 1956 RETMA chart. From a photograph of the system's digital reproduction of this image, it was concluded that there is negligible geometrical distortion in the image.

3.4. Uniformity

To experimentally determine uniformity of the SEC tube and telescope optical system, a defocussed, 5 $\times$ 5 arc min area of the quiet Sun near disk center was used to uniformly illuminate the faceplate. Normalized output signal distributions from digitized magnetograph data measured across the center of the tube in both horizontal and vertical directions indicate that in the vertical direction, the uniformity of tube response is within $\pm$ 10% over 90% of the center of tube and the signal intensity begins to roll off rapidly

as the edge of the scan area is approached. In the horizontal direction the tube response is flat within ± 10% over 80% of the tube, again rolling off rapidly toward the edge. In data analyses, effects of non-uniformities over the tube area can be nearly eliminated through use of photometric calibration data where intensity distributions over the entire field of view are obtained for quiet Sun illumination.

3.5. Lag

The image lag or retention in the SEC vidicon was measured by exposing the tube to obtain the normal operating signal level, turning off the photocathode voltage so that no additional signal could reach the target, and scanning the tube three consecutive times. The signal level of the second readout was approximately 15% of the level of the first readout, and the third was 5% of the first. Since scanning with the read beam has the same effect whether or not the output current is subsequently digitized, one re-scan (a total of two scans) between images adequately prepares the tube, as noted in Section 3.9.

3.6. Resolution

The resolution of the magnetograph system is determined by the system raster of 128 lines in the vertical direction and by the 128 discrete elements in the horizontal direction. Using the Kell factor (Fink, 1940) of 0.70 for the 5 × 5 arc min field of view the spatial resolution of a magnetogram is 3.3 arc sec; for the 2.0 × 2.0 arc min field it is 1.3 arc sec.

To experimentally investigate system resolution, the digital response of the system to a Westinghouse resolution chart was displayed using the system's greyscale monitor. Examination of a photograph of this display indicates that line pairs four pixels or greater in width can be resolved easily. As the line pair width diminishes and nears the size of two pixels, the resolution is determined by the line pairs position relative to the affected pixels: lines centered on elements are clearly resolvable, whereas those centered midway between elements are not resolved.

3.7. Signal-to-noise

Calculations of the signal-to-noise ratios (S/N) of the various components of the analog and digital systems give individual S/N values from which the system's overall S/N can be estimated. As an example, the SEC vidicon S/N is calculated from the number of photoelectrons produced per picture element (pixel) per exposure and has been estimated at ~ 400 for the MSFC optical system. For the preamplifier the estimated rms noise level is 175 pA (Section 2.2.2) and the upper limit for the signal current is 100 nA, so that for this component the S/N of the brightest elements is given by

$$(S/N)_p = 100\ \text{nA}/175\ \text{pA} = 570\ .$$

The theoretical equivalent S/N for the vidicon and preamp chained together thus would be approximately 335. In fact, the S/N of the camera and preamplifier was measured experimentally at the output of the camera video amplifier using the composite video signal produced by a flat field illumination with a signal output current of 100 nA; using

the formula (Hall, 1971)

$$S/N = 6(CE - CD)/CD\,,$$

where CE and CD are the signal and noise envelopes, respectively, the resultant S/N is 114 : 1.

Other components in the magnetograph system will add to the noise, and for some of these it is difficult to estimate a S/N factor. Consequently, we have devised an experimental technique from which we can determine the S/N of the total system. In this technique, we assume that the noise level from each pixel derives from two distinct sources: a true random (rms) noise and a 'fixed pattern' noise caused by the variation of response of the vidicon target surface (non-uniformity across the vidicon). Results from various tests using this technique indicate a nominal signal-to-noise value of $\sim 100 : 1$ (rms) when operating voltages are optimized. Using the image enhancement capability of the system this S/N can be increased up to a factor of ~ 16 using the full 255 enhancements. Consequently, the theoretical magnetic sensitivity of this magnetograph is determined by an rms S/N of $\sim 1600 : 1$, which would permit measurements of ~ 4 G longitudinal fields and ~ 70 G transverse fields as determined from theoretical calibrations relating detected signal to magnetic field strength.

3.8. Zeiss filter performance characteristics

The magnetograph system utilizes a specially built Zeiss birefringent filter designed to have a bandpass of 0.125 at 525.022 nm. In December 1968 and again in May 1975 experimental verification of the optical characteristics of the Zeiss filter were undertaken at Kitt Peak National Observatory using the McMath solar telescope and spectrograph. Photoelectric scans of the filter transmission near the center of the Zeiss aperture were obtained with the Zeiss filter tuned to 525.120 nm in the solar continuum; the filter was then tuned to line center, 525.022 nm, where further photoelectric scans were obtained. From these data the experimental transmission profile of the filter was derived and is shown in Figure 3. Further results indicate that the transmission profile for the full aperture is quite similar to this and there are no appreciable changes in filter transmission characteristics as the filter is tuned over its entire range of 525.022 ± 0.80 nm. The theoretical transmission of a birefringent filter composed of N elements is given by

$$T(\lambda) = T_0 \prod_{k=0}^{N} \{\cos(\pi \Delta\lambda 2^{-k} d^{-1})\}^2\,,$$

where T_0 is the transmission at the center wavelength (λ_0) of the bandpass, $T(\lambda)$ is the transmission at a wavelength λ, $\Delta\lambda = \lambda - \lambda_0$, and d is a constant. If the final polarizing element of the filter is rotated through an angle δ, the transmission characteristics are then determined by the equation

$$T' = T\{\cos(\pi \Delta\lambda d^{-1} + \delta)\}^2\,.$$

By choosing $\delta = 0.85\pi$, a good fit to the experimental transmission profile is obtained, as is indicated in Figure 3. This analytical representation for the Zeiss filter has been

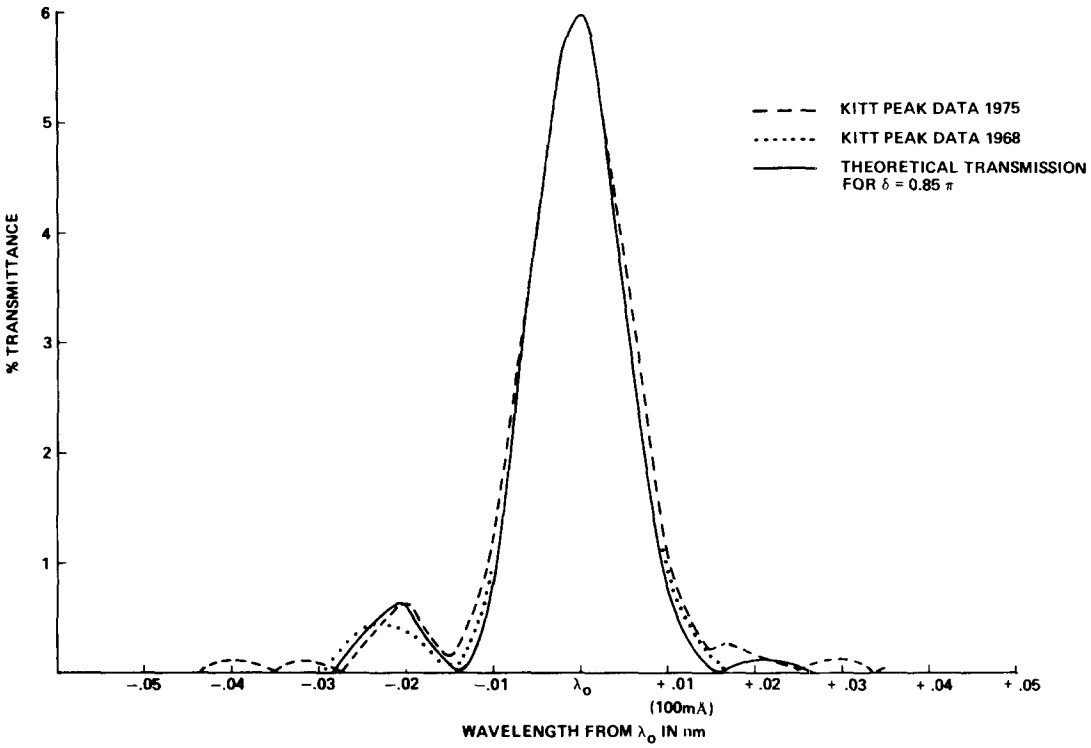

Fig. 3. Measured and theoretical transmission profiles for the $\frac{1}{8}$ Å-bandpass Zeiss birefringent spectral filter.

adopted for use in computer programs for the reduction and interpretation of the magnetograph data.

3.9. Retardation Measurements

The basic principle of operation of the MSFC magnetograph is the accurate analysis of the state of polarization of the incident solar intensity. This analysis is accomplished by introducing known retardations into the optical path by means of the two electro-optical crystals (potassium deuterium phosphate – KD*P's). Consequently, it is important to determine experimentally the performance of the KD*P's and to ascertain that each crystal is producing as nearly as possible the correct retardation in each of the six measurement sequences. In this section we outline the experimental techniques developed for these purposes and present results of several tests. In Figure 4, the relative orientation of the slow (s) axes of the two KD*P retarders together with the polarizing plane of the analyzer (A) are shown in the x, y, z coordinate system where $+z$ represents the direction of light propagation in the optical train. The axis x_0 designates a reference direction determined by the orientation of the transverse component of the measured solar magnetic field. In the analysis the three basic types of polarized light (Q, U, V) are defined in relation to the analyzer axis (A); these three parameters together with the total

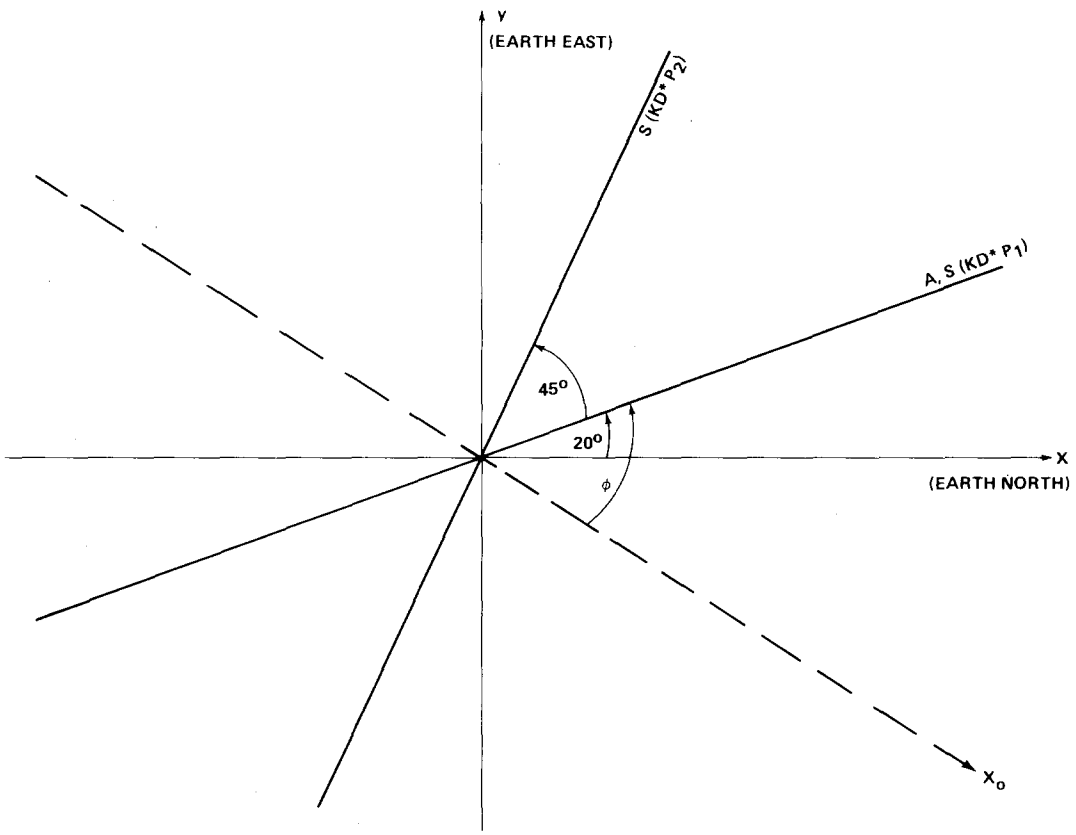

Fig. 4. Relative orientations of the KD*P retarders' slow axes and polarizer-analyzer axis with respect to image plane coordinates (Earth north and east).

intensity, I, comprise the Stokes vector which completely describes the intensity and state of polarization of a beam of light. In the operational sequences of the MSFC magnetograph, the Stokes intensities are transformed via the electro-optical retarders into light intensities linearly polarized parallel to the analyzer transmission axis; in this manner the complete polarization analysis of the incident beam is performed. This polarization analysis can be expressed mathematically by use of the Mueller matrices (Shurcliff, 1962) for the two KD*P retarders and the linear analyzer. If the retardations of the crystals KD*P_1 and KD*P_2 are designated δ_1 and δ_2, respectively, and if the linear analyzer's transmission axis is at an angle ϕ to the reference direction x_0, then the measured intensity in the ith sequence is given by

$$I_i = \tfrac{1}{2}\{I_0 + Q_0[\cos(\delta_2)_i \cos 2\phi - \sin(\delta_1)_i \sin(\delta_2)_i \sin 2\phi] + \\ + U_0[\cos(\delta_2)_i \sin 2\phi + \sin(\delta_1)_i \sin(\delta_2)_i \cos 2\phi] + \\ + V_0[\cos(\delta_1)_i \sin(\delta_2)_i]\}\,, \quad i = 1, 2, \ldots, 6\,. \tag{1}$$

In this equation the Stokes parameters for linear polarization, Q_0 and U_0, are defined with respect to the directions x_0 and z which are determined by the direction of the magnetic field and line-of-sight, respectively. In Table I, we show a hypothetical 'analysis' in which it is assumed the retarders perform perfectly; the six sequences represent the actual operational configurations of the MSFC system. To complete this hypothetical analysis the case of a homogeneous magnetic field must be assumed so that the Stokes parameter U_0 may be set to zero (Unno, 1956), and the parameters I_0, Q_0, and V_0 as well as the azimuth ϕ can be calculated readily from sums and differences of the I_i.

TABLE I

Operational sequences of electro-optical retarders

Sequences (i)	KD*P$_1$	KD*P$_2$	Output intensity I_i
1	0	$+\lambda/4$	$\frac{1}{2}(I_0 + V_0)$
2	0	$-\lambda/4$	$\frac{1}{2}(I_0 - V_0)$
3	$+\lambda/4$	$+\lambda/4$	$\frac{1}{2}(I_0 - Q_0 \sin 2\phi + U_0 \cos 2\phi)$
4	$+\lambda/4$	$-\lambda/4$	$\frac{1}{2}(I_0 + Q_0 \sin 2\phi - U_0 \cos 2\phi)$
5	0	0	$\frac{1}{2}(I_0 + Q_0 \cos 2\phi + U_0 \sin 2\phi)$
6	0	$+\lambda/2$	$\frac{1}{2}(I_0 - Q_0 \cos 2\phi - U_0 \sin 2\phi)$

In actual practice the analysis is complicated by variations of the retardances $(\delta_1)_i$ and $(\delta_2)_i$ from their ideal values. Thus it is necessary to measure the actual retardances introduced and their variations over the field of view. This is accomplished by operating the system in the six sequences while introducing known states of polarized light into the optical beam with the insertion of a linear polarizer and a quarterwave plate. If these known polarization states are described relative to the analyzer axis direction A, the transmitted intensity is derived from Equation (1) with $\phi = 0$:

$$I_i = \tfrac{1}{2}\{I + Q\cos(\delta_2)_i + U\sin(\delta_1)_i \sin(\delta_2)_i + V\cos(\delta_1)_i \sin(\delta_2)_i\} \,. \qquad (2)$$

Using this expression we can analyze the measured intensities of the six operational sequences of the system (see Table I) in each of the six experimental tests performed in this 'cross-talk' analysis as outlined in Table II.

TABLE II

Cross-talk analysis tests

Test description	Stokes parameter	Measured intensity
1. Linear polarizer parallel to A	$+Q$	$\frac{1}{2}I[1 \pm \cos(\delta_2)_i]$, $i = 1, \ldots, 6$.
2. Linear polarizer perpendicular to A	$-Q$	
3. Linear polarizer at $+45°$ to A	$+U$	$\frac{1}{2}I[1 \pm \sin(\delta_1)_i \sin(\delta_2)_i]$, $i = 1, \ldots, 6$.
4. Linear polarizer at $-45°$ to A	$-U$	
5. Linear polarizer at $+45°$ to $\lambda/4$ plate	$+V$	$\frac{1}{2}I[1 \pm \cos(\delta_1)_i \sin(\delta_2)_i]$, $i = 1, \ldots, 6$.
6. Linear polarizer at $-45°$ to $\lambda/4$ plate	$-V$	

TABLE III

Retardation measurement results

Sequence (i)	δ_1		δ_2	
	Measured	Ideal	Measured	Ideal
1	−0°.14	0°	91°.52	+90°
2	+0°.43	0°	−87°.75	−90°
3	87°.81	90°	90°.20	+90°
4	90°.22	90°	−89°.76	−90°
5	(1)	0°	+2°.73	0°
6	(2)	0°	+177°.89	180°

In Table III we present typical results obtained on 22 October 1976; the values indicated are obtained from an average of several pixels at the center of the field of view (on the optical axis).

The excellent agreement between theoretical and measured retardations indicated by these results cannot be obtained over the entire field of view of the MSFC magnetograph. This problem is a consequence of the natural birefringence of the KD*P crystals wherein the phase retardance is different for different optical paths through the crystal. For light rays on or near the optic axis of the system, the collimator renders the beam parallel to this axis. However, for off-axis point sources in the 5 × 5 arc min field of view, the light from each point will be collimated but the collimated beams will be inclined relative to each other. Since the optic axes of the KD*P's are aligned experimentally to be perpendicular to the center of the aperture, the maximum deviations in retardances occur from points at the corners of the square field of view. In Figure 5a, we show the theoretically calculated variations in retardation over the 5 × 5 arc min field of view. From the retardation tests of 22 October 1976, we calculated the errors in retardations of both KD*P crystals in all six sequences. Figure 5b shows contour levels of the retardation errors for $KD^*P_{1,2}$ in sequences 3 and 4 (Table I); positive and negative contours represent $\pm 5°$ error increments outward from the center of the field of view.

Because of these non-negligible errors in the retardances away from the center of the field of view, one of the authors (E.A.W.) has designed and installed a magnesium fluoride (MgF_2) correction plate between the two KD*P crystals. Since MgF_2 and KD*P are, respectively, positive and negative uniaxial crystals, the field-of-view errors in retardation introduced by the KD*P can be reduced substantially by a properly designed and aligned MgF_2 plate. In Figure 5c measured contour levels of retardation errors at $\pm 5°$ increments are again shown for the KD*P sequences of Figure 5b, but in this case a MgF_2 correction plate has been added to the KD*P optical package. As can be seen by comparing Figures 5b and 5c the maximum variation of retardance over the 5 × 5 arc min field of view has been reduced from $\pm 25°$ (where the central retardance is 90°) to $\pm 5°$. Consequently, the original data reduction scheme can be used with only small corrections required for the extreme corners of the field of view. A more detailed discussion of how the MgF_2 plate expands the field of view of two KD*P's can be found elsewhere (West, 1978).

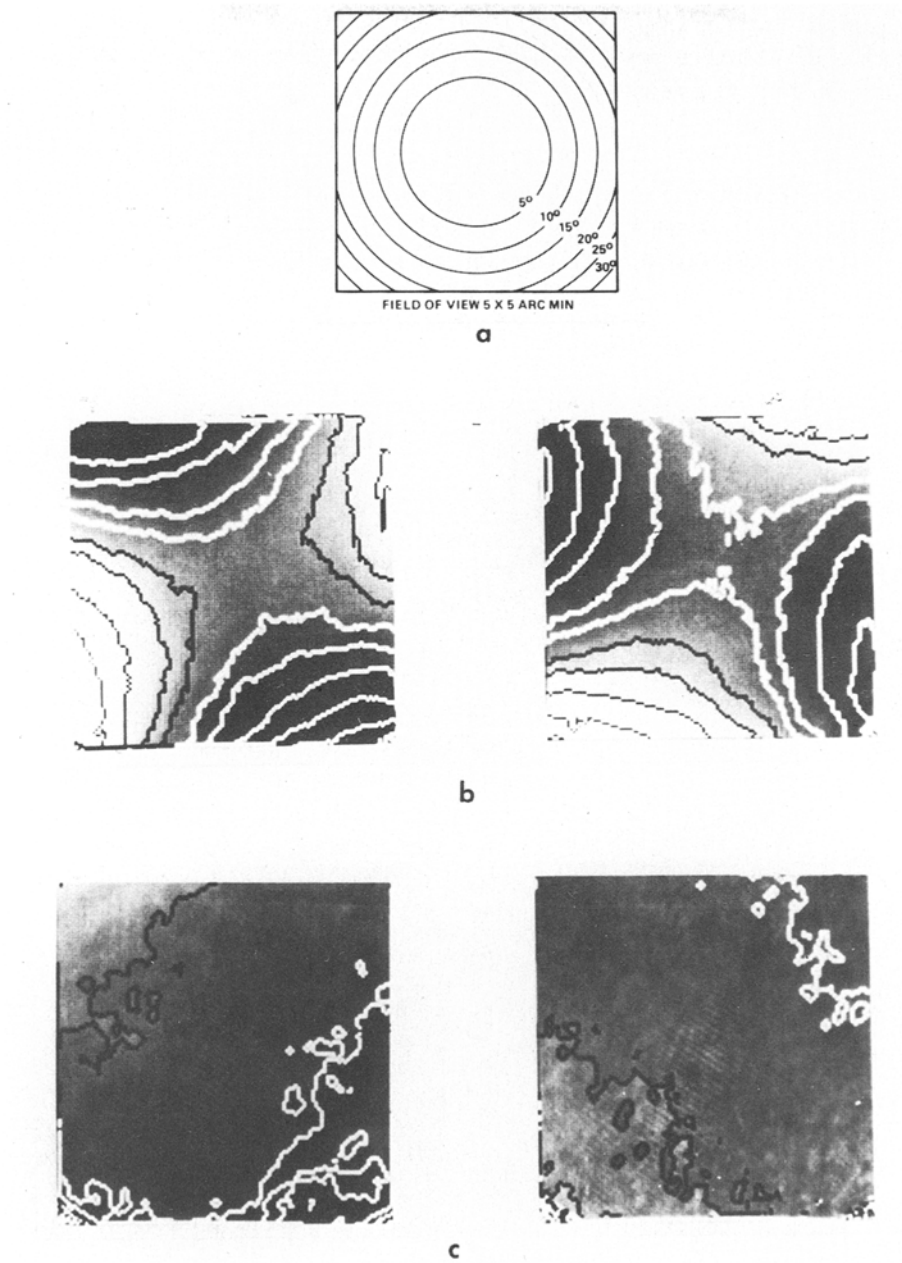

Fig. 5. Retardation errors of KD*P crystals over 5 × 5 arc min field of view. (a) Theoretical variations. (b) Measured variations without MgF_2 correction plate; positive (negative) contours delineate $+5°$ ($-5°$) error intervals increasing outward from center; *left*: $KD*P_2$ at $\lambda/4$; *right*: $KD*P_1$ at $+\lambda/4$. (c) Same as (b) but with MgF_2 correction plate.

A further factor in the performance of the KD*P crystals is the temperature dependence of the dc voltage applied to a crystal to obtain a given retardance. This variation is described by the linear relation

$$V_1 = V_{RT}(T_1 - T_c)/(T_{RT} - T_c),$$

where V_1 is the halfwave voltage of the KD*P temperature T_1, V_{RT} is the halfwave voltage at the room temperature T_{RT}, and T_c is the Curie temperature (200 K). In Figure 6 we illustrate this linear variation of voltage with temperature and indicate the experimentally

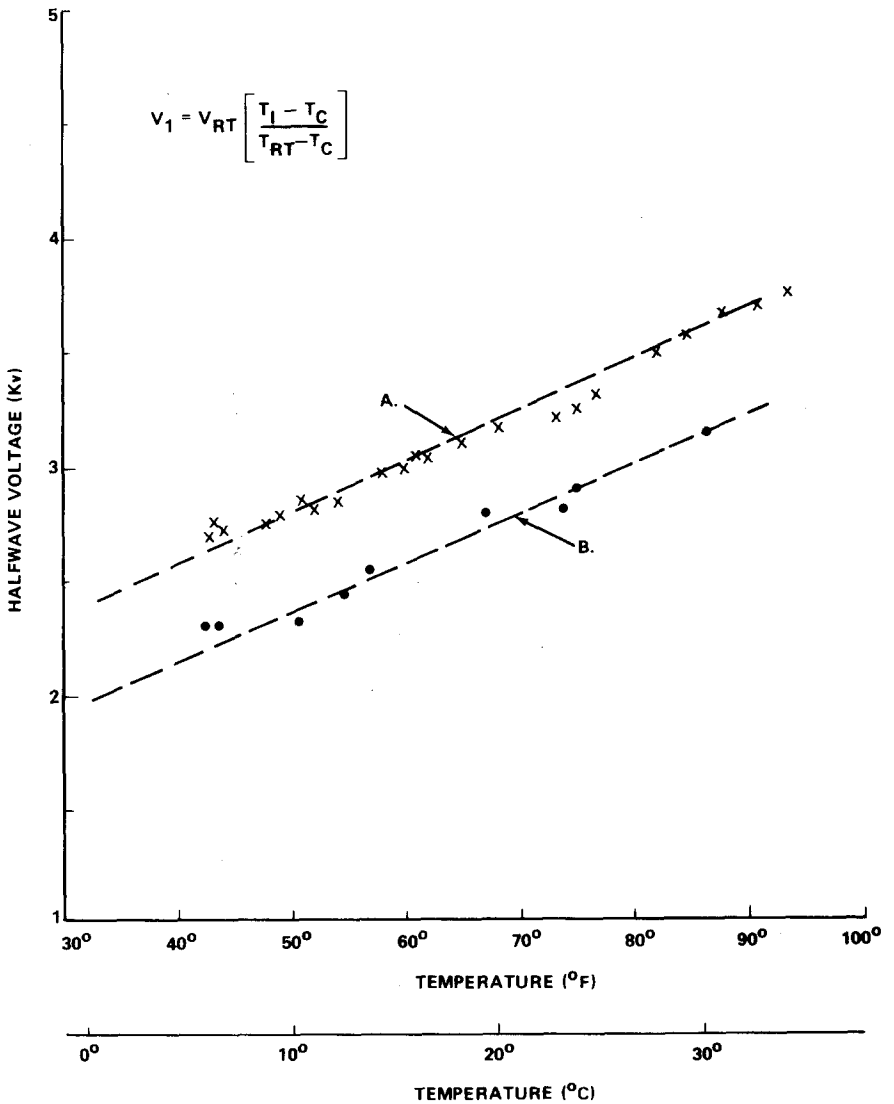

Fig. 6. Measured linear variation of KD*P halfwave retardation voltage with temperature for two (A, B) KD*P crystals.

measured data for two different KD*P crystals. To guarantee that the voltages which are applied to the two KD*P crystals during operation of the system produce the correct retardations, a temperature controller is attached to the crystals.

3.10. Polarization calibration

The ultimate test of the reliability and accuracy of the MSFC magnetograph system is the comparison of measured polarizations with values expected when known levels of linearly and circularly polarized intensities are introduced into the optical beam. Figure 7 illustrates results obtained for the U and Q Stokes parameters when linear polarization was produced by rotating a polarizer in front of the polarizing optics. Three separate data sets were obtained for each curve representing zero, one and two vidicon re-scans (erasures) between successive exposures. These results indicate the problem of vidicon 'stickiness' whereby the measured polarization is only 75 to 80% of the expected value for the case of no re-scans. If one re-scan is introduced, in the case of low and intermediate values of percent polarization, the measured signal is approximately 95% of the true value, and this is probably within the accuracy of the experimental technique of producing the polarized light. The saturation of the measured polarization at approximately 87%, regardless of the number of re-scans, when 100% polarization (theoretically) is introduced, is attributed to residual intensities in the 'low' signal due to improper setting of the a/d bias voltage and to incomplete extinction by the crossed polarizers. However, these problems occur for very high levels of % polarization which are not encountered in measurements of linear and circular polarizations produced by solar magnetic fields: calculations based on penumbral, plage and photospheric models indicate that polarization levels are limited to 40% or less regardless of the magnetic field strength. Thus, results from tests such as these indicate that data taken with no vidicon re-scans will need to be calibrated, but if re-scans are introduced, the measured polarization levels will be reliable. Furthermore, it appears that one re-scan should be sufficient to achieve this degree of reliability.

4. Scientific Applications

In this section we discuss some of the specific scientific investigations which utilize the unique capability of this magnetograph system to map the full magnetic vector over an entire active region with high temporal resolution.

Studies of vector field morphology in active regions are performed using data formats illustrated in Figure 8 where an enlarged portion of the 5 × 5 arc min field of view of AR 2776 has been plotted. These data were part of a vector sequence obtained 35 min prior to the 2B flare which began 7 November 1980 at 17 : 24 UT and peaked at 17 : 41 UT. In this vector sequence 14 separate vector magnetograms were obtained with a time resolution of 4.5 min using an exposure time of 1/15 s (a better time resolution of 1.75 min is obtained utilizing the fastest exposure rate of 1/60 s under optimum conditions). These data illustrate a transverse field configuration which has been observed for several flare-productive regions: the azimuth of the transverse field is

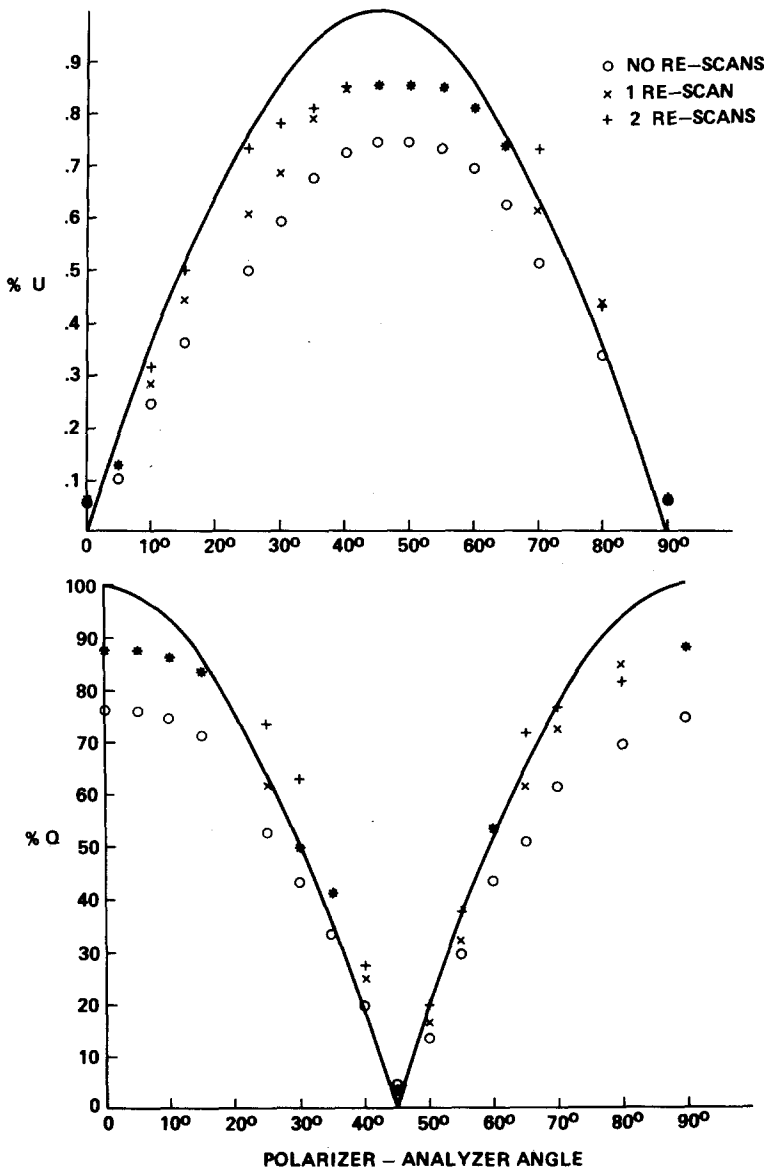

Fig. 7. Measured linear polarization compared with expected (theoretical) values.

aligned ~ parallel to the neutral line of the longitudinal field along the portion between points 1 and 2 and below.

In generating numerous plots such as these we have gained further insight into the sensitivity and accuracy of our vector field measurements. Experience gained, for example, in setting the lower limits on positive and negative contours in the 'longitudinal' plots indicates that the lowest detectable percent circular polarization is ~ 0.1% which

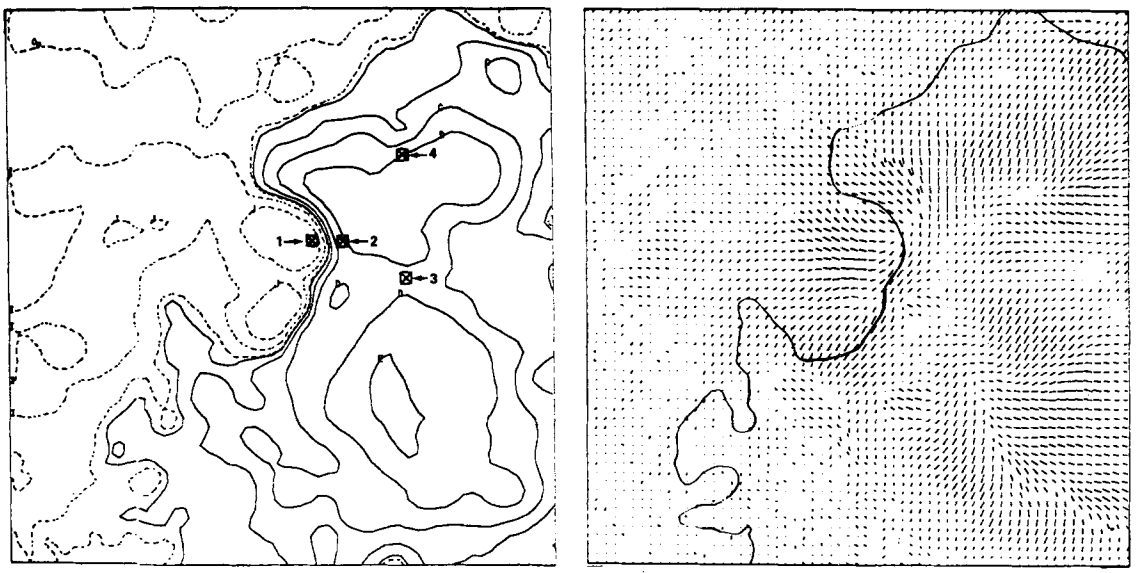

(a) (b)

Fig. 8. Vector magnetograms of AR2776 on 7 November 1980 at 16:43 UT over a 2.3′ × 2.3′ field. (a) Longitudinal magnetic field. (b) Orientations of the transverse azimuth angle with the longitudinal neutral line superimposed.

represents a line-of-sight, quiet-photospheric field of ~ 4 G. Similarly, to eliminate noisy background in 'transverse' plots we generally choose linear polarization cut-offs at 0.16% (although some particularly good data sets have been contoured to 0.10%); this translates into a transverse field strength of ~ 90 G for a penumbral model atmosphere. The accuracy of the azimuth angle (ϕ) determination is best seen in results of our studies of magneto-optical effects. In these analyses values of ϕ for a given position in a sunspot are plotted as a function of the Zeiss filter position in the spectral line. For field strength regions where Faraday rotation is not evident, these plots should give a good representation of the reproducibility of the azimuth calculation, and indeed, they indicate a variation of $\leq \pm 5°$.

Under flaring conditions very rapid data rates can be initiated for higher time resolution. For the November 7 flare a 'flare mode' was started for the period 17:31–18:06 UT in which vector magnetograms were obtained at 2-min intervals using an exposure rate of 1/15 s. From these data temporal variations of the vector field during the flare can be investigated for the most intense Hα flare points (points 1 and 2 in Figure 8) as well as for locations away from the flare (points 3 and 4).

To obtain unambiguous quantitative data, for example, to study the magnitude and orientation of vector fields in sunspots, rapid data sequences are obtained stepping the filter bandpass through the spectral line at 0.0010 nm steps. In Figure 9 measured circularly polarized intensities are shown as a function of wavelength for a pixel in the umbra of AR2776 (point 4 in Figure 8). Also shown is the deconvolved V-Stokes intensity which was obtained using the measured filter bandpass profile in an FFT

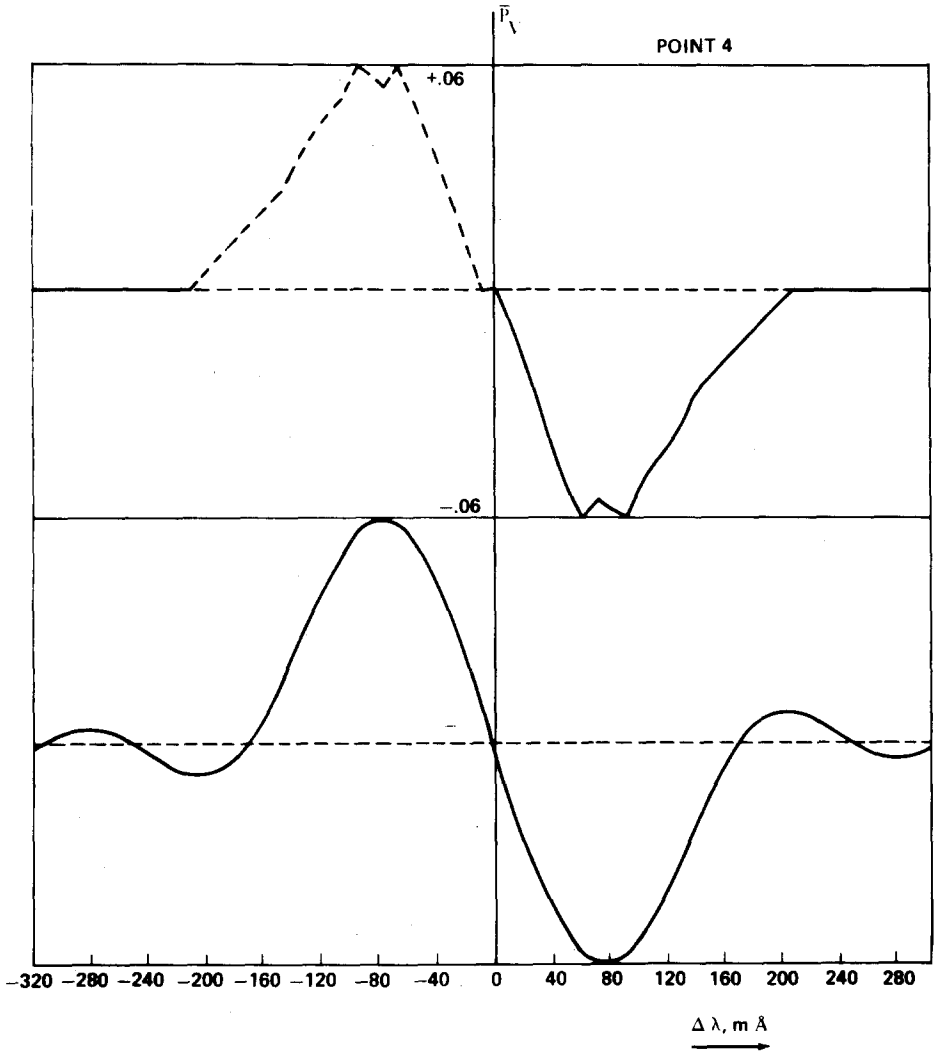

Fig. 9. Results of a line profile scan taken in circularly polarized light for the point 4 in Figure 8. *Upper curve*: fractional circular polarization $\bar{P}_v$; *lower curve*: deconvolved V-Stokes profile.

program. The measured wavelength separation of the peak from line center is 78.8 mÅ which corresponds to a field strength of 2040 G; Mt. Wilson data show a value of 2100 G in this area.

From quantitative analyses such as these, data can be generated for use in various theoretical models, for example, to calculate potential and force-free fields (Hagyard and Teuber, 1978), compute the magnetic energy content of active regions using the general force-free formulation of Molodensky (1974) (see Krall and Hagyard, 1980), analyze chromospheric responses to footpoint shears of a magnetic loop based on a 3-component, non-planar magnetohydrodynamic model of Wu *et al.* (1981, private communication), and calculate vertical electric current distributions through the photosphere (Krall *et al.*, 1981).

References

Fink, D. G.: 1940, *Principles of Television Engineering*, Mc-Graw-Hill, New York.

Hagyard, M. J. and Teuber, D.: 1978, *Solar Phys.* **57**, 267.

Hall, J. A.:1971, in L. M. Biberman and S. Nudelman (eds.), *Photoelectronic Imaging Devices*, Plenum Press, New York.

Honeycutt, R. K. and Burkhead, M. S.: 1973, in J. W. Glaspey and G. A. H. Walker (eds.), *Astronomical Observations with Television-Type Sensors*, Proceedings of Symposium at University of British Columbia, Vancouver, B.C., Canada.

Krall, K. R. and Hagyard, M. J.: 1980, *Bull. Am. Astron. Soc.* **12**, 899.

Krall, K. R., Smith, J. B., Hagyard, M. J., West, E. A., and Cumings, N. P.: 1981, *Solar Phys.* **79**, 59.

Molodensky, M. M.: 1974, *Solar Phys.* **39**, 393.

Shurcliff, W. A.: 1962, *Polarized Light*, Harvard University Press, Cambridge, MA.

Unno, W.: 1956, *Publ. Astron. Soc. Japan* **8**, 109.

Walker, G. A. H., Auman, J. R., Buchholz, V. Z., Goldberg, B. A., Gower, A. C., Isherwood, B. C., Knight, R., and Wright, D.: 1972, *Advances in Electron Physics*, Vol. 33b, Academic Press, New York.

West, E. A.: 1978, *Appl. Opt.* **17**, 3010.